Synthesis, mechanical characteristics, and gamma-ray attenuation of nickel phosphate glass loaded with barium

A. M. Al-Baradi [a], Kh. S. Shaaban [b,*]
[a] *Department of Physics, College of Science, Taif University, P.O. Box 11099, Taif 21944, Saudi Arabia*
[b] *Department of Chemistry, College of Science, Al-Azhar University, P.O. 71524, Assiut, Egypt*

A new formulation of BaO-NiO- P_2O_5 glass system was fabricated by conventional melt-quenching method with the molecular composition (17+*x*) BaO-(3-*x*)NiO-80P_2O_5 (*x* = 0; 0.5; 1; 2; and 3 mol%). The density improved from 3.39 to 4.27 g/cm^3, and the molar volume decreased from 41.85 to 33.78 cm^3/mol. The integrated BaO expanded the longitudinal velocity (4050–4290 ms^{-1}) and shear velocity (2119–2285 ms^{-1}). The elastic modulus (GPa) expanded with the increase of BaO. These results indicate possible uses for dynamic building glass design since they demonstrate that the physio-elastic qualities depend on composition. The PNBa-20 has the highest Z_{eff}, followed by PNBa-19.5, PNBa-19, PNBa-18, and PNBa-17 has the lowest values. Therefore, Z_{eff} of the PNBa glasses increased in the order: PNBa-20> PNBa-19.5> PNBa-19> PNBa-18> PNBa-17. The $\sum R$ of the PNBa glasses increased in the order: PNBa-20> PNBa-19.5> PNBa-19> PNBa-18> PNBa-17. Thus, they are helpful in γ-ray shielding and other neutron absorption processes.

(Received April 1, 2025; Accepted July 21, 2025)

Keywords: BaO Glass, Elastic moduli, Radiation shielding

1. Introduction

Oxide glasses are adaptable materials with a wide range of applications due to their outstanding properties [1-3]. These glasses provide significant functional qualities, including electrical insulation, transparency, and mechanical strength, which are crucial for everyday use in electronics, optics, and construction. By combining different oxides, it is possible to improve the structural, mechanical, and radiation-shielding properties of the glass. This capability allows for the development of specialized glasses that meet the specific needs of various industries [4-6]. As technology advances, glass fabrication will remain a dynamic field, with ongoing research focused on discovering new compositions and processing techniques to improve the performance and functionality of glass materials [7-9]. Phosphate glasses are garnering significant interest due to their unique combination of properties [9-10].

Glasses based on transition metal oxides (TMOs) are highly valuable for various applications due to their unique properties. By adjusting the type and amount of TMOs in the glass matrix, their mechanical, structural, and radiation shielding qualities can be fine-tuned. TMO-containing glasses are known for their thermal stability and resistance to chemical degradation, making them suitable for harsh environments [11-15]. Additionally, TMO-based glasses like nickel oxide (NiO) exhibit semiconducting properties, making them useful in electronic and photovoltaic devices [16].

Barium-doped glasses have garnered significant interest, with researchers investigating the effects of BaO on various properties across different glass systems. Recently, many studies have concentrated on the mechanical and radiation-shielding of phosphate glasses that contain BaO. BaO acts as a modifier oxide in the NiO-P_2O_5 glass system, significantly altering the glass network. The focus is on evaluating how BaO doping alters the properties of NiO-P_2O_5 glass.

* Corresponding author address: khamies1078@yahoo.com
https://doi.org/10.15251/DJNB.2025.203.831

2. Materials and methods

Using the standard melting method, a series (17+x) BaO-(3-x)NiO-80P_2O_5 ($0 \leq x \geq 3$)glasses were fabricated. After being weighed, the precursors—$NH_4H_2PO_4$ (99.98%), $BaCO_3$ (98.5%), and NiO (98.5%) were mixed for two hours in an agate mortar. They were then heated to 300 °C, 600 °C, and 1150 °C to eliminate ammonia (NH_3), (H_2O), and CO_2, and melted the mixture. After that, the melt is quickly quenched onto plates made of stainless steel. For 5 hours, the obtained glass samples were placed in an oven that had been preheated to a temperature higher than 350 °C in order to remove internal stress and stop the glass from breaking. The glass compositions (17+x) BaO-(3-$_x$)NiO-80P_2O_5 are listed in Table 1 under the designation PNBax.

The Archimedes method is a well-recognized technique for measuring the density (ρ) as:

$$\rho = 0.863x\left(\frac{W_a}{W_{xylene}}\right) \tag{1}$$

The relative error of (ρ) is ±0.0025 g/cm^3. The volume of the glass sample (V_m) can be determined as:

$$V_m = M/\rho, \tag{2}$$

Oxygen packing densities (OPD) and oxygen molar volume (OMV) were computed as follows:

$$OMV = \left(\frac{M}{\rho}\right)\left(\frac{1}{\sum xini}\right) \tag{3}$$

$$OPD = \left(\frac{1000\,C}{Vm}\right)\left(\frac{Mol}{L}\right) \tag{4}$$

A Matec 8020 Ultrasonic Data Acquisition System was used to perform ultrasonic measurements at room temperature using the pulse superposition technique (Matec Instruments, USA). The relative error is ±0.1% and the velocity is ±5 ms^{-1}. The following standard relations were used in the calculation of elastic moduli.

$$\text{Longitudinal } L = \rho v_l^2, \tag{5}$$

$$\text{Transverse, } G = \rho v_t^2 \tag{6}$$

$$\text{Young's modulus, } Y = (1+\sigma)2G \tag{7}$$

$$\text{Bulk modulus, } K = L - \left(\frac{4}{3}\right)G \tag{8}$$

$$\text{Micro-hardness, H} = \frac{(1-2\sigma)\text{Y}}{6(1+\sigma)}. \tag{9}$$

$$\text{Debye temperature, } \theta_D = \frac{h}{k}\left(\frac{9N}{4\pi V_m}\right)^{\frac{1}{3}} M_s \tag{10}$$

$$\text{Average ultrasonic velocities,M}_\text{s} = \frac{1}{3}\left(\left(\frac{1}{\text{v}_\text{l}^3}\right) + \left(\frac{2}{\text{v}_\text{t}^3}\right)\right)^{-\frac{1}{3}} \tag{11}$$

$$\text{Thermal expansion, } \propto_P = 23.2\,(V_L - 0.57457) \tag{12}$$

$$\text{Acoustic impedance, Z} = \rho * 1000 * \text{v}_\text{T} \tag{13}$$

The packing density (V_i) and dissociation energy (G_i) can be used to estimate the elastic moduli using the Makishima-Mackenzie model (MMM) [17–18] as follows:

$$V_i = (\frac{1}{V_m}) \sum V_i x_i \quad (14)$$

$$G_i = \sum G_i x_i \quad (15)$$

$$L = K + \left(\frac{4}{3}\right) G \quad (16)$$

$$G = \frac{30 V_i^2 G_i}{(10.2 V_i - 1)} \quad (17)$$

$$Y = 8.36 V_i G_i \quad (18)$$

$$K = 10 V_i^2 G_i \quad (19)$$

Radiation parameters for PNBa glasses can be assessed using the Phy-X code [19]. Effective atomic number,Z_{eff} computed as:

$$Z_{eff} = \frac{\sum_i F_i A_i (\mu/\rho) i}{\sum_i F_i \frac{A_i}{Z_i} (\mu/\rho) i} \quad (20)$$

Neutron radiation shielding can be assessed with [19] and computed as:

$$\left(\frac{\Sigma_R}{\rho}\right) = \sum_i w_i \left(\frac{\Sigma_R}{\rho}\right)_i \quad (21)$$

$$R = \sum_i \rho_i \left(\frac{R}{\rho}\right)_i \quad (22)$$

Table 1. Glass compositions mol %.

code	P_2O_5	NiO	BaO
PNBa-17	80	3	17
PNBa-18	80	2	18
PNBa-19	80	1	19
PNBa-19.5	80	0.5	19.5
PNBa-20	80	0	20

3. Results and discussion

3.1. Density (ρ), molar volume (V_m), and related parameters

Fig. 1 shows the (ρ g/cm³) and (V_m) with varying BaO contents. Fig. 1 demonstrates that the (ρ) increases from 3.39 to 4.27 as the amount of BaO increases, whereas the (V_m) decrease from 41.85 to 33.78. Replacing the lighter NiO with the weightier BaO molecules led to a rise in (ρ). As an outcome, glass becomes more denser and compact [20-23].

Increased BaO content reduces the average distance ($d_{Ba\text{-}Ba}$, 10^{-8}) between barium atoms, changing from 5.8 to 5.5 cm. The inter-nuclear distance (ri) decreases from 8.74 to 7.72 cm, and the polaron radius (r_P) decreases from 2.51 to 2.22 cm. The deviation of $d_{Ba\text{-}Ba}$, rp, and ri is illustrated in Fig. 2. The decline in $d_{Ba\text{-}Ba}$ levels with increasing BaO concentration results in a rise

in ion concentration (N_i) from $2.45 \times 10^{21}$to 3.57×10^{21} ions/cm^3. The field strength (F) around the Ba ions increases from 3.17×10^{15} to 4.1×10^{15} due to these enhanced interactions. Fig. 3 illustrated the (N_i) and (F) of PNBa glasses [24-28].

The (OMV) and (OPD) changed when the amount of BaO in the glass structure increased. The increase in (ρ) with growing BaO results in a rise in (OPD) from 100.4 to 124.35. The decline in (V_m) results in a decline in (OMV) from 10 to 8.04. Fig. 4 illustrated the (OMV) and (OPD) of PNBa glasses [29-31].

3.2. Mechanical investigations

Table 2 displays the experimental ultrasonic velocity (V_L& V_T) measurements for the glass system, while Fig. 5 displays the results. The table 2 and Fig. 5 show that the (V_L& V_T) and the concentration of BaO are correlated. As the amount of BaO in the glasses under examination increased, the V_L and V_T rose from 4050 to 4290 and 2119 to 2285 m/s, respectively. As BaO is added to glass interstices, the network's closure rate increases. As a result, the network becomes more rigid or the glass structure is strengthened. It is clear that there is an increase in both V_L & V_T. BaO acts as the glass modifier, filling in the gaps between molecules and creating densely packed connectivity throughout the network. This can be described by the (ρ), of the glass. As the ρ of the glasses increase, their velocities also increase [32-36].

Increasing the elastic modulus (GPa) of PNBa glass increases rigidity. The increase in BaO concentration, as shown in Table 2 and Fig. 6, shows an increase in the values of all elastic moduli. *L* increases from 55.6 to 78.58, *G* increases from 15.2 to 22.29, *K* increases from 35.31 to 48.86, and *Y* increases from 39.93 to 58.05. The increase in BaO content contributes to the improvement of glass network density, and the tensile force increases continuously. From these results, it can be concluded that Ba-doped glass strengthens the connection [36-39].

Fig. 7 and Table 2 show the H rises with the BaO, from 1.91 to 2.94 GPa. The rise in H is due to the rise in the (ρ) and the compactness of the glass. In addition, Fig. 7 and Table 2 show that the Z value increases from 7.2×10^{-6} to 9.8×10^{-6} with the increase of BaO concentration. The increase of Z value is caused by the increase of V_T and ρ. Fig. 8 and Table 2 show that the M_s& θ_D increases with the increase of BaO concentration, from 1644 to 1770 m/s, and from 312 to 361 K respectively. This increase is related to the increment in the V_L&V_T.

Table 3 and Fig. 9 show the calculated values of V_i& G_i for the synthesized PNBa-17-PNBa-20 glass samples. It was observed that the highest value of V_i for PNBa-20 followed by PNBa-19.5, PNBa-19, PNBa-18, and PNBa-17, in opposite the highest value of G_i for PNBa-17 followed by PNBa-18, PNBa-19, PNBa-19.5, and PNBa-20. This observation is due to the difference in the V_i& G_i between BaO and NiO. This improvement is due to structural changes in the glass matrix that work in concert.

The addition of BaO increases the observed variations in all elastic moduli [17-18], as shown in Table 3 and Fig. 10. L_{th} increases from 120.3 to 169, G_{th} increases from 34.7 to 41.5, K_{th} increases from 74.1 to 113.6, and Y_{th} increases from 85.2 to 105.3. In particular, adding BaO increases the glass's stiffness and improves its resistance to deformation under stress. The alterations in atom arrangement, bonding patterns, and general cohesion within.

Table 2. The values of, ultrasonic velocities and other mechanical parameters.

code	PNBa-17	PNBa-18	PNBa-19	PNBa-19.5	PNBa-20
V_L	4050	4115	4193	4234	4290
V_T	2119	2140	2194	2231	2285
L	55.6	61.6	69.09	72.42	78.59
G	15.2	16.7	18.92	20.109	22.29
K	35.31	39.41	43.87	45.613	48.86
Y	39.93	43.8	49.6	52.596	58.05
H	1.91	2.06	2.38	2.58	2.94
α_p(K^{-1})	93946.67	95454.67	97264.27	98215.47	99514.67
θ_D(K)	312	322	338	346	361
M_s	1644	1660	1702	1730	1770
Z*10^{-6}	7.2	7.8	8.6	9.0	9.8

Table 3. The values of mechanical parameters as [17-18].

code	PNBa-17	PNBa-18	PNBa-19	PNBa-19.5	PNBa-20
V_i (cm^3/mol)	0.73	0.78	0.83	0.86	0.90
G_i (kJ/cm^3)	14.02	14.00	13.98	13.97	13.96
L_{th}	120.3	133.3	149.1	155.2	169.0
G_{th}	34.7	36.6	38.9	39.7	41.5
K_{th}	74.1	84.5	97.3	102.2	113.6
Y_{th}	85.2	90.9	97.5	99.9	105.3

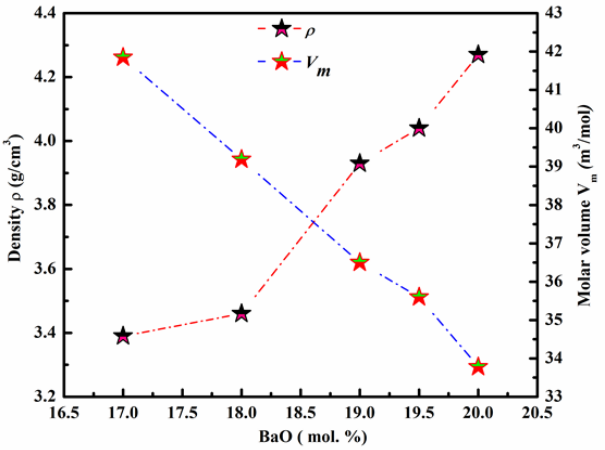

Fig. 1. (ρ) and (V_m), of the PNBa samples.

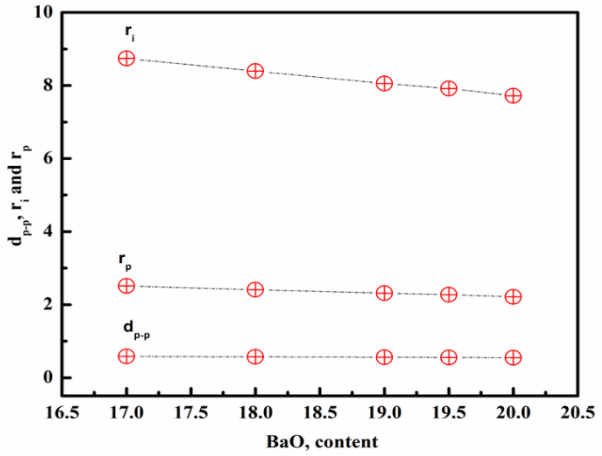

Fig. 2. $d_{Ba\text{-}Ba}$, rp, and ri of the PNBa samples.

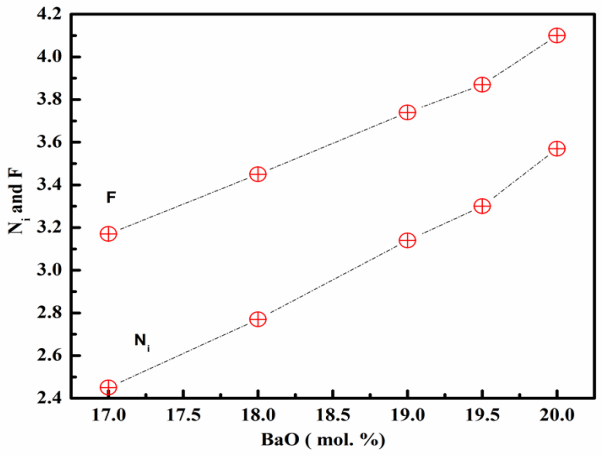

Fig. 3. (N_i) and (F) of PNBa samples.

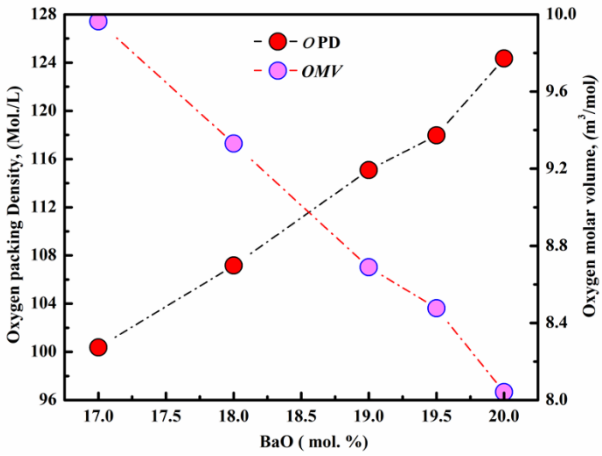

Fig. 4. (OMV) and (OPD) of PNBa samples.

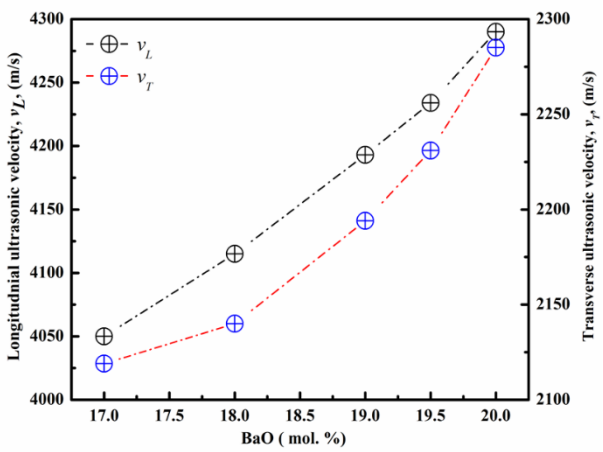

Fig. 5. (V_L& V_T) of PNBa samples.

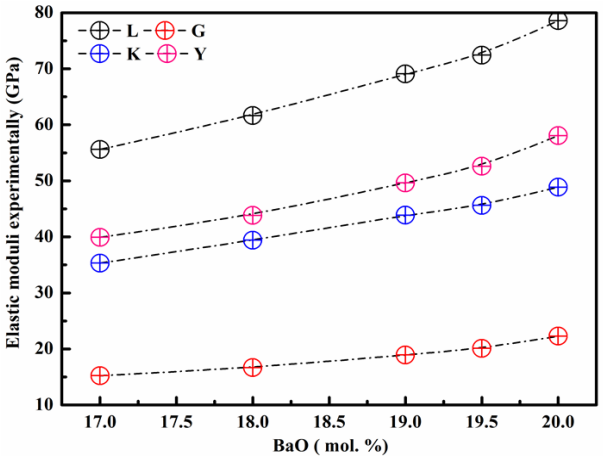

Fig. 6. Elastic moduli of PNBa samples.

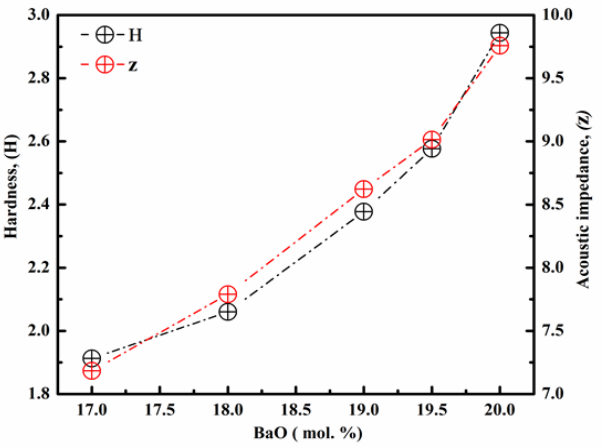

Fig. 7. H& Z of PNBa samples.

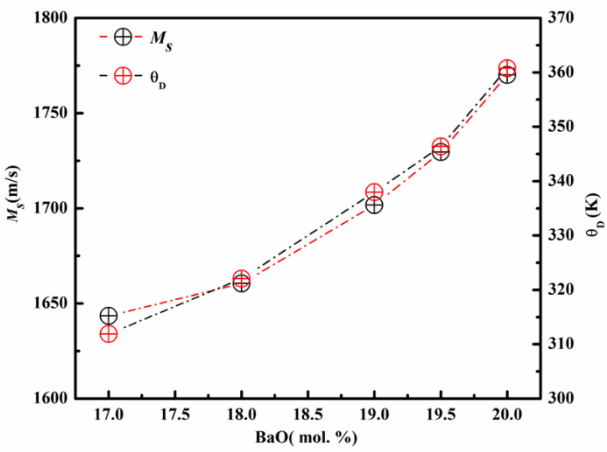

Fig. 8. M_s& $\theta_D$of PNBa samples.

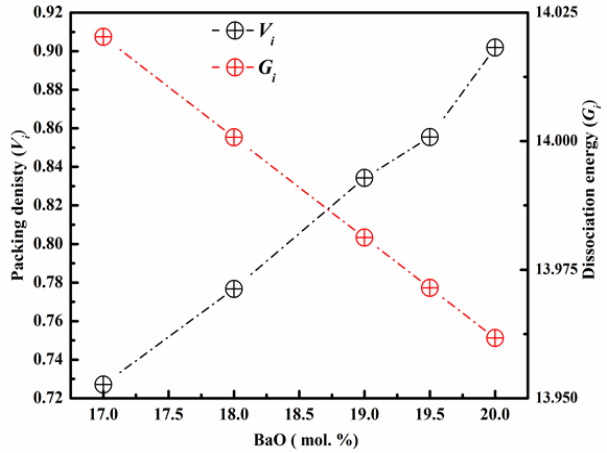

Fig. 9. V_i& $G_i$of PNBa samples.

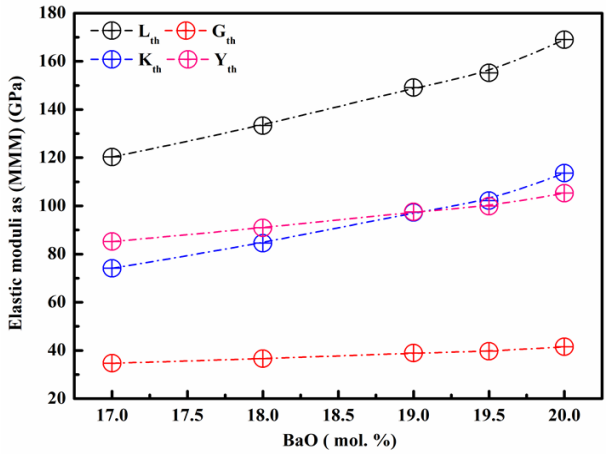

Fig. 10. Elastic moduli of PNBa glasses as (MMM) [17-18].

3.3. Gamma radiation shielding properties

Fig. 11 displays the Z_{eff} at various γ −ray energies. The value of Z_{eff} varies from 13.84 to 26.86 for PNBa-17, from 13.98 to 27.36 for PNBa-18, from 14.12 to 27.86 for PNBa-19, from 14.2 to 28.1 for PNBa-19.5, and from 14.27 to 28.35 for PNBa-20. There were some notable variations, though. For all glasses, the maximum Z_{eff} happens at 40 keV while, the minimum occurs at 1.5 MeV. These variations are associated with changes in the chemical compositions concerning photon interaction mechanisms. Therefore, Z_{eff} of the PNBa glasses increased in the order: PNBa-20> PNBa-19.5> PNBa-19> PNBa-18> PNBa-17. According to Fig. 11, PNBa-20 has the highest Z_{eff}, followed by PNBa-19.5, PNBa-19, PNBa-18, and PNBa-17 has the lowest values. The reason behind this trend is that PNBa-20 has a higher density than other glasses, which improves the material's capacity to interact with radiation. Furthermore, the Zeff exhibits a decreasing trend as the γ-ray energy increases, suggesting that the PNBa glasses work better at lower γ-ray energies [36-39].

3.4. Neutron shielding properties

Fig. 12 displays the removal cross-sections of the PNBa-17, PNBa-18, PNBa-19, PNBa-19.5, and PNBa-20 for fast neutrons. The total $\sum R$ cm^{-1} for the PNBa-17, PNBa-18, PNBa-19, PNBa-19.5, and PNBa-20 glasses are: 0.107, 0.114, 0.123, 0.126, and 0.133. This demonstrates a steady improvement in the glasses' capacity to slow down fast neutrons. The rise in the partial density and removal cross-section of Ni and O atoms is responsible for the observed increase. Hence, $\sum R$ of the PNBa glasses increased in the order: PNBa-20> PNBa-19.5> PNBa-19> PNBa-18> PNBa-17. Thus, they are helpful in shielding and other neutron absorption processes.

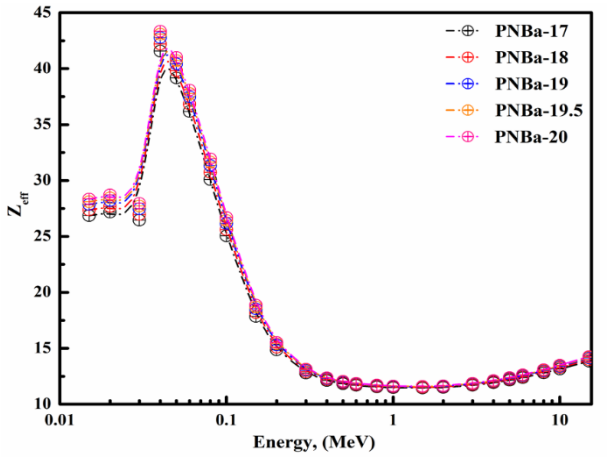

Fig. 11. Z_{eff} of PNBa glasses.

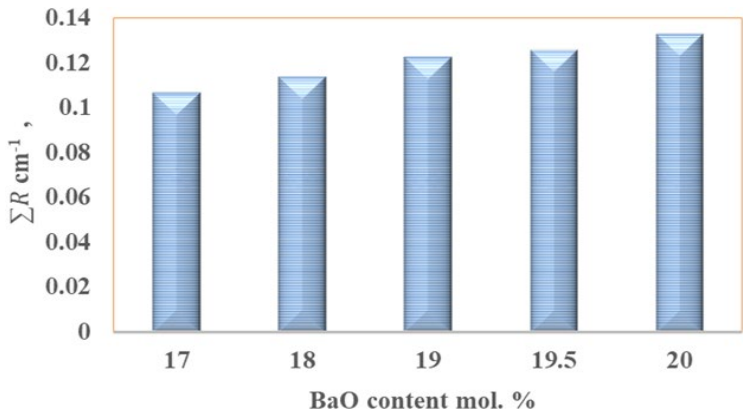

Fig. 12. ∑ Rof PNBa glasses.

4. Conclusions

The PNBa glass system was successfully prepared by using melting and quenching techniques. Based on the results, increasing BaO content raised the ρwhile decreasing the V_m. As the amount of BaO in the glasses under examination increased, the V_L and V_T rose from 4050 to 4290 and 2119 to 2285 m/s, respectively. The values of all elastic moduli are increased: L increases from 55.6 to 78.58, G increases from 15.2 to 22.29, K increases from 35.31 to 48.86, and Y increases from 39.93 to 58.05. From these results, it can be concluded that Ba-doped glass strengthens the connection.

The addition of BaO increases the observed variations in all elastic moduli according (MMM): L_{th} increases from 120.3 to 169, G_{th} increases from 34.7 to 41.5, K_{th} increases from 74.1 to 113.6, and Y_{th} increases from 85.2 to 105.3. The PNBa samples have the potential to be used in dynamic architectural glass designs. The PNBa-20 has the highest Z_{eff}, followed by PNBa-19.5, PNBa-19, PNBa-18, and PNBa-17 has the lowest values. Therefore, Z_{eff} of the PNBa glasses increased in the order: PNBa-20> PNBa-19.5> PNBa-19> PNBa-18> PNBa-17. The $\sum R$ of the PNBa glasses increased in the order: PNBa-20> PNBa-19.5> PNBa-19> PNBa-18> PNBa-17. Thus, they are helpful in γ-ray shielding and other neutron absorption processes.

Acknowledgments

The authors express their gratitude Taif University Researchers Supporting Project number (TU-DSPP-2024-124), Taif University, Taif, Saudi Arabia.

References

[1] Shaaban, K., Al-Baradi, A. M., Ali, A. M., Alotaibi, B., Journal of Materials Research and Technology, 18, 1909-1921, (2022); https://doi.org/10.1016/j.jmrt.2022.03.090
[2] Shaaban, K.S., B.M. Alotaibi, Nuha Alharbi, Z.A. Alrowaili, M.S. Al-Buriahi, Sayed A. Makhlouf, A.F. Abd El-Rehim, Radiation Physics and Chemistry,193, 109995, (2022); https://doi.org/10.1016/j.radphyschem.2022.109995.
[3] Shaaban, K.S., Al-Baradi, A.M. & Ali, A.M., J Mater Sci: Mater Electron **33**, 3297, (2022); https://doi.org/10.1007/s10854-021-07530-w
[4] Almuqrin, A.H., Mahmoud, K.A., Wahab, E.A.A. et al, Eur. Phys. J. Plus **136**, 639 (2021); https://doi.org/10.1140/epjp/s13360-021-01564-z
[5] Shaaban, Kh. S., Al-Baradi, Ateyyah M., Aloraini, Dalal Abdullah., Radiochimica Acta, (2025); https://doi.org/10.1515/ract-2024-0356
[6] Shaaban, K.S., Alomairy, S., Al-Buriahi, M.S., J Mater Sci: Mater Electron **32**, 26034, (2021); https://doi.org/10.1007/s10854-021-05885-8
[7] Ali, A.M., Alrowaili, Z.A., Al-Baradi, A.M. et al., Silicon **14**, 6447, (2022); https://doi.org/10.1007/s12633-021-01440-6
[8] Alsafi, Khalid, Aloraini, Dalal Abdullah, Saif, M. A. and Shaaban, Kh. S., Radiochimica Acta, 112, (9), 703, (2024); https://doi.org/10.1515/ract-2024-0272
[9] Shaaban, K.S., Alrowaili, Z.A., Al-Baradi, A.M. et al., Silicon 14, 6457–6465, (2022); https://doi.org/10.1007/s12633-021-01441-5
[10] Sayed, M.A., Basha, B., Al-Harbi, N. et al., Eur. Phys. J. Plus, **138**, 455, (2023); https://doi.org/10.1140/epjp/s13360-023-04079-x
[11] Shaaban, K. S., Aloraini, D. A., Alsafi, K., Almutairi, H. M., Al-Saleh, W. M., Alzahrani, A. S., Materials Today Communications, 38, 108309, (2024); https://doi.org/10.1016/j.mtcomm.2024.108309
[12] Shaaban, K.S., Ateyyah M. Al-Baradi, B.M. Alotaibi, A.F.Abd El-Rehim, Journal of Materials Research and Technology,23, 756, (2023); https://doi.org/10.1016/j.jmrt.2023.01.062.

[13] El-Maaref, A.A., Alotaibi, B.M., Alharbi, N. et al. J Inorg Organomet Polym **32**, 3117, (2022); https://doi.org/10.1007/s10904-022-02345-6
[14] Shaaban, K.S., Al-Baradi, A.M., Ali, A.M. Silicon **14**, 8971, (2022); https://doi.org/10.1007/s12633-022-01702-x
[15] Basha B., Shaaban, K.S., Abdel Wahab E.A., Digest Journal of Nanomaterials and Biostructures 18, (2), 713, (2023); https://doi.org/10.15251/DJNB.2023.182.713
[16] E. A. Allam, R. M. El-Sharkawy, Kh.S. Shaaban, A. El-Taher M. E. Mahmoud, Y. El Sayed, Digest Journal of Nanomaterials and Biostructures, 17, (1), 161, (2022); https://doi.org/10.15251/DJNB.2022.171.161
[17] A. Makishima, J.D. Mackenzie, Direct calculations of Young modulus of glass, J. Non-Cryst Solids, 12, 35, (1973); https://doi.org/10.1016/0022-3093(73)90053-7
[18] A. Makishima, J.D. Mackenzie, Calculation of Bulk modulus, shear modulus and Poisson's ratio of glass, J. Non-Cryst. Solids 17, 147, (1975); https://doi.org/10.1016/0022-3093(75)90047-2
[19] Şakar E, Özpolat ÖF, Alım B, Sayyed MI, Kurudirek M, Radiation Phys Chem **166**: 108496, (2020); https://doi.org/10.1016/j.radphyschem
[20] Shaaban, K.S., Alyousef, H.A., El-Rehim, A.F.A., Silicon **14**, 12001, (2022); https://doi.org/10.1007/s12633-022-02124-5
[21] Shaaban, K.S., Alotaibi, B.M., Alharbiy, N. et al. Silicon **14**, 11991, (2022); https://doi.org/10.1007/s12633-022-02029-3
[22] Wahab, E.A.A., Shaaban, K.S., Al-Baradi, A.M., Silicon **14**, 4915, (2022); https://doi.org/10.1007/s12633-021-01236-8
[23] Almutairi, H.M., Aloraini, D.A., Alsafi, K. Al-Saleh W. M., Alzahrani A. S., Shaaban, K. S., Silicon **16**, 2873, (2024); https://doi.org/10.1007/s12633-024-02900-5
[24] Shaaban, K.S., Al-Baradi, A.M., Ali, A.M. Silicon **14**, 10375, (2022); https://doi.org/10.1007/s12633-022-01783-8
[25] Althagafi, T.M., Sayed, M.A., Alghasham, H.A. Nuha Al-Harbi, Kh. S. Shaaban, Silicon **15**, 7047, (2023); https://doi.org/10.1007/s12633-023-02567-4
[26] Aloraini, D.A., Ashour, A., Shaaban, K.S. Silicon **16**, 1837, (2024); https://doi.org/10.1007/s12633-023-02804-w
[27] Sayed, M.A., Basha, B., Al-Harbi, N. Shaaban, K. S., Silicon, **15**, 6463, (2023); https://doi.org/10.1007/s12633-023-02537-w
[28] Alghasham, H. A., Ismail, Y. A., Aloraini, D. A., Shaaban, K., Materials Today Communications, **38**, 107840, (2024); https://doi.org/10.1016/j.mtcomm.2023.107840
[29] Shaaban, K.S., Al-Baradi, A.M., Wahab, E.A.A, Silicon, **14**, 5057, (2022); https://doi.org/10.1007/s12633-021-01309-8
[30] Al-Baradi, A.M., Wahab, E.A.A., Shaaban, K.S. Silicon **14**, 5277, (2022); https://doi.org/10.1007/s12633-021-01286-y
[31] Shaaban, K.S., Alotaibi, B.M., Al-Baradi, A.M. Yousef El Sayed, Ashour A., Silicon **15**, 4409, (2023); https://doi.org/10.1007/s12633-023-02351-4
[32] Mahrous, Eman M., Al-Baradi, Ateyyah M., Shaaban, Kh. S., Radiochimica Acta, (2024); https://doi.org/10.1515/ract-2024-0307
[33] Al-Baradi, A.M., Alotaibi, B.M., Alharbi, N. A.F.Abd El-Rehim, Shaaban, K.S, Silicon **14**, 10391, (2022); https://doi.org/10.1007/s12633-022-01801-9
[34] Shaaban, K.S., Alsafi, K., Aloraini, D.A. Wafa M. Al-Saleh, Haifa M. Almutairi, E. E. Assem. Silicon **16**, 2899, (2024); https://doi.org/10.1007/s12633-024-02897-x
[35] El-Rehim, A.F.A., Zahran, H.Y., Yahia, I.S., Wahab, E.A.A., Shaaban, K.S., Journal of Materials Engineering and Performance 30, 1872, (2021); https://doi:10.1007/s11665-021-05513-w
[36] Alsafi, K., Ismail, Y. A., Aloraini, D. A., Almutairi, H. M., Al-Saleh, W. M., Shaaban, K. S. Progress in Nuclear Energy, **170**, 105151, (2024); https://doi.org/10.1016/j.pnucene.2024.105151
[37] Shaaban, K. S., Althagafi, T. M., Ashour, A., Alalawi, A., Al-Buriahi, M., Ibraheem, A. A. Radiation Physics and Chemistry, **216**, 111440, (2024); https://doi.org/10.1016/j.radphyschem.2023.111440
[38] Shaaban, K. S., Aloraini, D. A. Materials Research Bulletin, 184, 113266. (2025); https://doi.org/10.1016/j.materresbull.2024.113266

[39] Shaaban, K.S., Aloraini, D.A., Al-Baradi, A.M. et al. Silicon, (2025); https://doi.org/10.1007/s12633-024-03217-z